Models for Branching Networks in Two Dimensions

Leah Edelstein-Keshet, Bard Ermentrout

SIAM Journal on Applied Mathematics, Volume 49, Issue 4 (Aug., 1989), 1136-1157.

SIAM J. APPL. MATH.
Vol. 49, No. 4, pp. 1136-1157, August 1989

010

MODELS FOR BRANCHING NETWORKS IN TWO DIMENSIONS*

LEAH EDELSTEIN-KESHET† AND BARD ERMENTROUT‡

Abstract. In this paper mathematical models for branching networks growing in one and two dimensions are described. Continuum equations are formulated to represent evolving spatial distributions of density given a variety of assumptions about branching and crosslinking kinetics. In accommodating the influence of angular branch distributions, a set of integropartial differential equations are obtained.

It is found that crosslinking (which eliminates apical growth) acts as a density-regulating mechanism. If the branching angle φ is small, this mechanism further leads to a phenomenon of orientation selection: It is shown analytically that for small φ a spatially homogeneous network with an initial uniform distribution of branch orientations will align along a single axis as a result of instability of the uniform steady state to small perturbations that are nonuniform in the angular variable. Because instability first occurs to a mode $e^{il\theta}$ for which $l=2$, such networks eventually contain only parallel branches.

Similar phenomena lead to a transition in properties of spatially propagating networks, whose angular distributions are diffuse for $\varphi > 0.29$ and sharply defined for $\varphi < 0.24$. Other properties of propagating networks, including traveling wave behavior, are described analytically and illustrated by numerical simulations.

Key words. branching networks, growth by branching, crosslinking branch orientations, pattern formation

AMS(MOS) subject classifications. primary 92; secondary 35, 34, 70

1. Introduction.

Motivation for studying branching networks arises from their prevalence in biological, chemical, and physical systems. Network structures occur in plant architecture, long chain polymers, drainage channels, fracture lines in solids, and other systems [23], [16], [10]. All of these are dynamic structures that change and evolve as they grow in space, whether in one or several dimensions. How such changes occur, and what inherent properties of the network lead to its eventual shape is a question we will explore in this paper.

Networks in which *crosslinks* occur between neighboring branches form a special subclass of branching systems. (In biological situations this process is called *anastomosis.*) Typical examples of networks that have crosslinks are the vascular systems, neural networks [20], as well as organisms such as hydroids and fungi [18], [15]. Connections between branches or filaments have several physiological purposes. For example, neural synapses transmit signals, the close proximity of capillary tips allows for the circulation of the blood, whereas fusions between hyphae (in mycelial fungi) or stolons (in hydroids) permit the exchange and transport of internal substances, nuclei, and organelles. Thus, in biological networks, it has been the accepted dogma that the significance of crosslinking is chiefly a mechanism for communication between adjoining parts of the network. Aside from such physiological roles, crosslinking can play an important role as a mechanism that regulates growth and development of form in a network [6]-[9].

To summarize key ideas, consider the events underlying the formation of a network. If growth is apical (i.e., confined to tips of branches), the number of growing apices

* Received by the editors April 18, 1988; accepted for publication (in revised form) September 27, 1988.

† Mathematics Department, University of British Columbia, Vancouver, British Columbia V6T 1Y4, Canada. The work of this author while a visitor at Duke University was supported by National Science Foundation grant DMS-86-01644 and by a Duke University Research Council minor grant 453-4123.

‡ Department of Mathematics, University of Pittsburgh, Pittsburgh, Pennsylvania 15260. The work of this author was supported by National Science Foundation grant DMS-87-01405.

determine how much growth takes place. Further, the location of apices determines where density is accumulating and thus influences the spatial distribution of the network. Crosslinking can play a regulatory role in the formation of a network because it leads to selective elimination of apices that will then cease to contribute to further growth.

Previous work (cited above) has been restricted to models of one-dimensional networks in which the direction of growth was along a single axis. In this paper our main aim is to extend the models and their analysis to higher dimensions where the phenomena are geometrically more complex. For example, as will emerge in the results, in two and three dimensions the orientations of branches can influence pattern formation because neighboring branches that are mutually transverse are more likely to come into contact and form crosslinks rather than branches that are parallel.

The organization of this paper is as follows. In § 2 we briefly review terminology and describe the phenomena. For a basic framework, the simplest one-dimensional models are then summarized in § 3. We then discuss the factors that enter into consideration in higher dimensions (for example, branch orientation) and derive the relevant equations in § 4. Analytical and numerical results on several simplified versions of such models are described in §§ 5 and 6.

2. Terminology and description of the phenomena. We restrict attention to branching structures that grow *apically*, i.e., in which filaments elongate only at their terminal ends (*tips*, or *apices*). The elongation of a branch is equivalent to spatial translation of its tip. We further assume that branches themselves are nonmotile, i.e., are attached to a substratum (in one and two dimensions), and that apices move in straight lines at a constant rate.

Branching is the process by which new apices are formed. There are several ways in which this can happen: *lateral branching* means that the new branch issues from some point along the length of the pre-existing branch. In *dichotomous branching*, an apex bifurcates, and is then replaced by two (or more) new tips. To avoid lengthy notation we refer to these two branching types by the letters F and Y, respectively, which are geometrically similar to the event they portray (see Fig. 1).

Crosslinking or anastomosis results in the fusion of an apex with a filament (*tip-to-branch anastomosis*) or with another apex (*tip-to-tip anastomosis*). Since, thereafter the fused apex can no longer grow, crosslinking is an event that eliminates apices. The letters H and W will be used to describe the above two types of crosslinking.

3. Branching and growth in one dimension. In this section we consider networks that grow in a single direction. An example of this type is a structure called a *strand* that is found in some filamentous fungi. This ropelike network consists of numerous filaments growing side by side, and held together by a gluey substance. The strand can thus grow for considerable distances as a one-dimensional structure. Both anastomosis and branching occurs between the adjacent filaments.

The following continuum model approximates the growth of densely branched networks assuming apical growth. For a simplified situation, consider only networks that are homogeneous along the y and z directions and grow in the x direction with all branches parallel to the x axis. We define the following:

$\rho(x, t)$ = total length of branches within some unit volume at (x, t),

$n(x, t)$ = number of growing apices in a unit volume at (x, t),

$v(x, t)$ = rate of extension of an apex at (x, t) in length per unit time.

When a single apex extends at the rate v it "deposits" a total branch length of $v\Delta t$ in its trail during the time Δt. Similarly, n apices traveling as a group with velocity

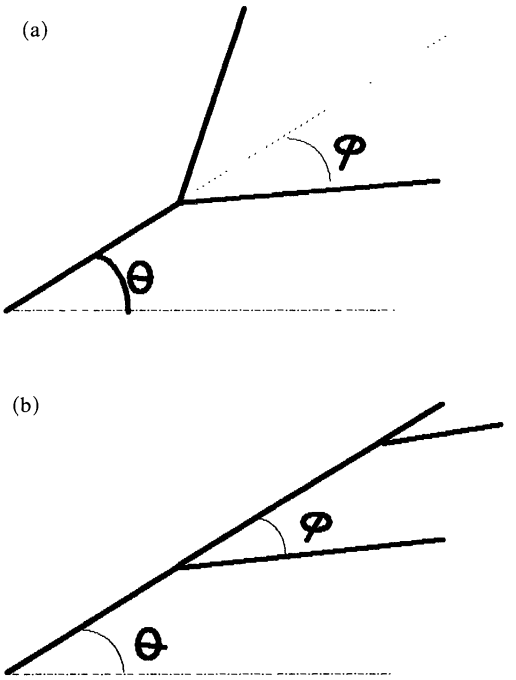

FIG. 1. *Branching can take place in two different ways.* (a) *In dichotomous (type Y) branching, a single tip produces two new tips.* (b) *In lateral (type F) branching, a new tip is produced somewhere along the length of the pre-existing branch. In the model that incorporates branch orientations, θ denotes the angle of orientation and φ is the branching angle.*

v deposit a total of $nv\Delta t$ units of length. Assuming a mortality of branches γ, this leads to the equation

$$\frac{\partial \rho}{\partial t} = nv - \gamma\rho, \tag{1}$$

for the density of branches.

An equation for apex density must take into account net motion of tips into and out of each location, as well as creation and elimination of tips. Defining

$\sigma_1(n, \rho)$ = branching rate (creation of apices per unit time per unit volume),

$\sigma_2(n, \rho)$ = crosslinking rate (elimination of apices per unit time per unit volume),

we obtain an equation of continuity

$$\frac{\partial n}{\partial t} = -\frac{\partial (nv)}{\partial x} + \sigma_1 - \sigma_2. \tag{2}$$

In (2), the term (nv), which is analogous to a convective flux, represents the rate of translation of apices in the x direction (extension of branches). In this paper we assume that v is constant. Equations (1) and (2), derived in [9], form a skeletal framework for one-dimensional continuum models of branching networks. These are semilinear hyperbolic partial differential equations. (Nonlinearity enters only via σ_i as described below.)

The appropriate mathematical forms for $\sigma = \sigma_1 - \sigma_2$ follow from mass action assumptions based on the kinetics of the underlying events. Since there are two pairs of possible events, as described in § 2, here we consider the four possible combinations of branching with crosslinking: *YH, FH, YW, FW.* The appropriate forms for σ_1 and σ_2 in each case are given in Tables 1 and 2. For example, *YH* corresponds to

$$\sigma(YH) = \sigma_1 - \sigma_2 = \alpha n - \beta n \rho \tag{3}$$

because Y-branching occurs only at apices (αn) and H-fusion is a second-order event, involving a "collision" between tips and branches ($\beta n \rho$).

The equations representing a *YH* network in one dimension are then

$$\frac{\partial \rho}{\partial t} = nv - \gamma\rho, \qquad \frac{\partial n}{\partial t} = -v\frac{\partial n}{\partial x} + n(\alpha - \beta\rho), \tag{4}$$

with spatially homogeneous steady states $(\rho, n) = [0, 0]$ and $[\alpha/\beta, \alpha\gamma/\beta v]$. As described previously in [7], traveling wave solutions to this set of equations satisfy

$$[\rho(x, t), n(x, t)] = [\rho(\xi), n(\xi)], \tag{5a}$$

where

$$\xi = x - ct, \tag{5b}$$

for c the velocity of the waves. This reduces the system to two ordinary differential equations:

$$\rho' = (\gamma\rho - vn)/c, \tag{6a}$$

$$n' = n(\beta\rho - \alpha)/[c - v]. \tag{6b}$$

It is an elementary calculation to show that for $c > v$, $[\alpha/\beta, \alpha\gamma/\beta v]$ is an unstable node or spiral, $[0, 0]$ is a saddle point, and there is a trajectory in the ρn plane joining $[0, 0]$ to $[\alpha/\beta, \alpha\gamma/\beta v]$. We remark that for $c < v$, such connections do not occur. This

TABLE 1
A summary of branching kinetics.

Branching type	Rate in 1D (σ_1)	Rate in 2D (σ_1)
Dichotomous (Y)	αn	$\alpha(n_- - n + n_+)$
Lateral (F)	$\alpha\rho$	$\alpha(\rho_- + \rho_+)$

TABLE 2
A summary of crosslinking kinetics.

Crosslinking type	Rate in 1D (σ_2)	Rate in 2D (σ_2)
Tip to branch (H)	$\beta n\rho$	$\beta n(x, \theta, t) \int_{-\pi}^{\pi} \rho(x, \theta', t) K(\theta - \theta')\, d\theta'$
Tip to tip (W)	βn^2	$\beta n(x, \theta, t) \int_{-\pi}^{\pi} n(x, \theta', t) K(\theta - \theta')\, d\theta'$

bounded heteroclinic trajectory represents the densities of ρ and n in the reference frame of the wave. Since the points $[0, 0]$ and $[\alpha/\beta, \alpha\gamma/\beta v]$ are attained only in the limits as $\xi \to \infty$, $\xi \to -\infty$, respectively, such waves represent networks in which there is material throughout the domain, not those whose densities have compact support. The wavespeed is larger than the extension rate of the tips because the phenomenon is a wave of branching, not a wave of particle motion. From the hyperbolic nature of equations (4) it is clear that if the initial density has compact support, the rate of outwards translation of the margin is $\mathbf{v}$.

From analysis of such one-dimensional models it emerges that for $\gamma = 0$ only a *YH*-network is *self-regulating,* in the sense that its density is bounded everywhere. (Other types have unbounded traveling wave solutions for $\gamma = 0$.) This means that in a *YH* network the intractions of branches suffices to control the local accumulation of density. Networks of the three other types tend to grow explosively and are only brought under control by branch mortality. See [7] for details and discussion of these results, [8] for an empirical test of the model in the context of filamentous fungi, [9] for a more detailed model incorporating transport of growth-essential substances, and [2] for a recent application to a model of tumor-induced capillary growth.

4. A model for oriented growth in two dimensions. For networks that grow and spread over two dimensions, the situation is more complicated. As previously mentioned in the Introduction, the geometry of the network then plays a significant role. For example, the likelihood that fusion will take place depends not only on the density, but also on the relative directions in which the branches are growing. Thus a model for networks in two or more dimensions must account for orientations as well as densities of branches.

In previous work by Edelstein-Keshet together with Segel (unpublished), an attempt was made to generalize the previous models by formulating vector equations for densities and apical growth rates. It was found that this approach was not suitable because the density of oriented branches cannot be added vectorially (parallel branches of opposite orientations do not "cancel"). In this paper we consider a more promising approach in which we redefine variables as distributions over an additional variable that represents orientation θ (see, for example, [1], [12] for similar ideas).

Consider the following new definitions of the variables for a two-dimensional network (note that these now depict orientation fields):

$\rho(\mathbf{x}, \theta, t)$ = total length (per unit area) of filaments oriented at angle θ at $(\mathbf{x}, t)$,

$n(\mathbf{x}, \theta, t)$ = total number (per unit area) of apices whose motion is oriented at angle θ at $(\mathbf{x}, t)$.

In the above it is to be understood that θ is an angle measured with respect to some fixed direction, for example, the x axis.

These definitions are made more technically precise in the following integral form:

$$\int_{\theta}^{\theta+\Delta\theta} n(\mathbf{x}, \theta', t)\, d\theta' = \text{the total number of tips moving in a direction subtending an angle } \theta \leqq \theta' \leqq \theta + \Delta\theta \text{ with the } x \text{ axis at location } \mathbf{x} \text{ and time } t.$$

A similar statement holds for $\rho(\mathbf{x}, \theta, t)$.

Now to derive an equation for ρ, note that filaments of orientation θ accrue as a result of the extension of apices whose direction of motion is θ. Thus

$$\frac{\partial \rho}{\partial t}(\mathbf{x}, \theta, t) = n(\mathbf{x}, \theta, t)v - \gamma\rho(\mathbf{x}, \theta, t), \tag{7}$$

where v is a (scalar) rate of extension and γ is mortality of branches. Note that by the above definitions, the (vector) velocity of apices $n(\mathbf{x}, \theta, t)$ is

$$\mathbf{v}(\theta) = (v \cos \theta, v \sin \theta). \tag{8}$$

This in turn implies that the flux of apices is

$$\mathbf{J}(\mathbf{x}, \theta, t) = n(\mathbf{x}, \theta, t)\mathbf{v}(\theta). \tag{9}$$

An equation of conservation for n will have the form

$$\frac{\partial n}{\partial t} = -\nabla \cdot \mathbf{J} + \sigma_1 - \sigma_2, \tag{10}$$

for $\nabla = (\partial/\partial x, \partial/\partial y)$, where now the terms σ_1 and σ_2 depend on orientation and on the orientation fields. In the following discussions we make assumptions about branching and crosslinking in two dimensions to derive the appropriate mathematical terms for σ_1 and σ_2.

4.1. How branching changes the orientation field: (deriving σ_1).

4.1.1. Dichotomous (Y) branching. Assume a fixed branching angle φ and a constant probability α, of branching. As an apex whose current direction of growth is θ bifurcates it produces two new tips whose orientations are $\theta \pm \varphi$. The parent tip is eliminated in the process (see Fig. 1(a)). Observe that every time a Y-branching event occurs, there is a tendency to increase the spectrum of orientations of the apices. The net accumulation of apices in the direction θ is then

$$\Delta n(\mathbf{x}, \theta, t) = \alpha[n(\mathbf{x}, \theta - \varphi, t) - n(\mathbf{x}, \theta, t) + n(\mathbf{x}, \theta + \varphi, t)]\Delta t, \tag{11}$$

where α is the branching rate. The first and last terms originate from the branching of parents oriented at $\theta \pm \varphi$ and the middle term accounts for disappearance of a parent tip of orientation θ when it branches. Denoting these terms by n_-, n, n_+, we note that

$$\sigma_1 = \frac{\Delta n}{\Delta t} = \alpha(n_- - n + n_+). \quad \text{(Type } Y\text{)} \tag{12}$$

In the case of small branching angle φ, this leads to an approximation derived by truncating a Taylor series expansion for n:

$$\sigma_1 = \mu \frac{\partial^2 n}{\partial \theta^2} + \alpha n, \tag{13}$$

for $\mu = \alpha\varphi^2$ and α, φ as defined above.

4.1.2. Lateral (F) branching. Assume that branching is lateral, takes place at rate α, and that the branching angle is φ (see Fig. 1(b)). Then the density of apices oriented in a direction θ increases when filaments with orientations $\theta \pm \varphi$ branch. Then by a similar reasoning we arrive at the expression

$$\Delta n(\mathbf{x}, \theta, t) = \alpha[\rho(\mathbf{x}, \theta - \varphi, t) + \rho(\mathbf{x}, \theta + \varphi, t)]\Delta t. \quad \text{(Type } F\text{)} \tag{14}$$

For small branching angles, a truncated Taylor series expansion for the above terms leads to the continuum approximation

$$\sigma_1 = \mu \frac{\partial^2 \rho}{\partial \theta^2} + 2\alpha\rho, \tag{15}$$

where, as before, $\mu = \alpha\varphi^2$.

4.2. How the orientation field affects crosslinking: (deriving σ_2).

4.2.1. Tip to branch anastomosis. Consider the situation shown in Fig. 2(a), (b). The configuration shown in (a) is unlikely to lead to contact and fusion between the apex and the neighboring branch, since their orientations are mutually parallel. In the configuration shown in Fig. 2(b), an obliquely oriented apex is moving toward the filament and will come into contact after a time $\tau = L/(v \sin \delta)$ where L is the distance of separation, $\delta = \theta - \theta'$ is the angle between the two branches, and v is the speed of motion (assumed fixed). The rate of fusion of apices of orientation θ, $n(\mathbf{x}, \theta, t)$, with filaments of orientation θ', $\rho(\mathbf{x}, \theta', t)$ is thus proportional to $\sin(\theta - \theta')$. In summing the contributions of branches oriented at all angles to fusions of tips with orientation θ, we obtain an integral of the form

$$\text{(16)} \qquad \text{likelihood of fusion of tip of orientation } \theta = \beta \int_{-\pi}^{\pi} \rho(\mathbf{x}, \theta', t) K(\theta - \theta')\, d\theta',$$

where β is the probability of crosslinking given that contact is established, and where the kernel K is typically

$$\text{(17)} \qquad K(\theta - \theta') \simeq C|\sin(\theta - \theta')| \qquad -\pi \leqq \theta \leqq \pi.$$

For the purposes of normalization take $C = \frac{1}{4}$. Then

$$\text{(18)} \qquad \int_{-\pi}^{\pi} K(\theta)\, d\theta = 1.$$

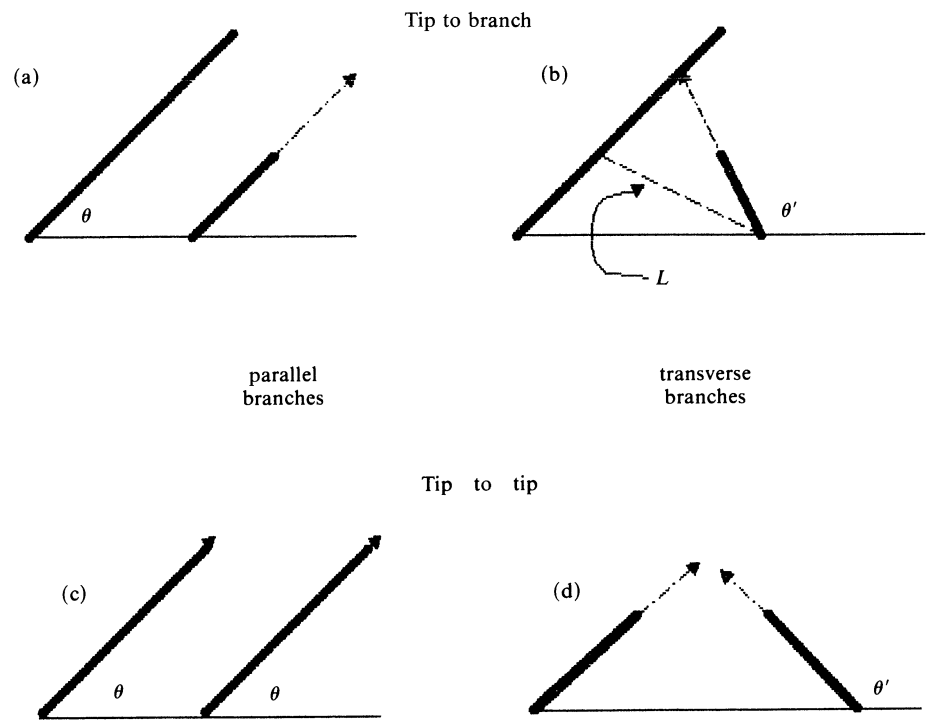

FIG. 2. *Crosslinking, or anastomosis, can occur in one of two ways. Top: a tip fuses with a branch (type H). Bottom: two tips fuse (type W). In both cases the probability of fusion is highest if the orientations of the elements are transverse ($\theta \neq \theta'$) as shown in* (b)*and* (d) *rather than parallel as in* (a), (c).

Thus σ_2 would be given by

$$\sigma_2 = \frac{\Delta n}{\Delta t} = -\beta n(\mathbf{x}, \theta, t) \int_{-\pi}^{\pi} \rho(\mathbf{x}, \theta', t) K(\theta - \theta')\, d\theta'. \tag{19}$$

4.2.2. Tip-to-tip anastomosis. Similar arguments based on Fig. 2(c), (d) lead to the conclusion that fusion of two tips can also be described by an integral term of the sort derived above. Since now the densities of apices only enter into consideration, we find that the term for σ_2 is

$$\sigma_2 = \frac{\Delta n}{\Delta t} = -\beta n(\mathbf{x}, \theta, t) \int_{-\pi}^{\pi} n(\mathbf{x}, \theta', t) K(\theta - \theta')\, d\theta', \tag{20}$$

with K as before.

A summary of kinetic terms representing branching and crosslinking in two dimensions are given in Tables 1 and 2. These terms are used below in the two-dimensional branching equations.

4.3. Two-dimensional branching equations. Putting together the terms derived in the previous sections we obtain four possible sets of equations for the four combinations of branching and crosslinking: *YH*, *FH*, *YW*, *FW*. A typical set that will be investigated in some detail is the *YH*-branching equations:

$$\frac{\partial \rho}{\partial t}(\mathbf{x}, \theta, t) = n(\mathbf{x}, \theta, t) v - \gamma \rho(\mathbf{x}, \theta, t), \tag{21a}$$

$$\frac{\partial n}{\partial t} = -\nabla \cdot \mathbf{J} + \alpha(n_- - n + n_+) - \beta n \int_{-\pi}^{\pi} \rho(\mathbf{x}, \theta', t) K(\theta - \theta')\, d\theta'. \tag{21b}$$

with $\mathbf{J}$ given by (9) and $n_\pm = n(\mathbf{x}, \theta \pm \varphi, t)$. While the equation for branch-density ρ is analogous to its one-dimensional counterpart, the above equation for the density of apices is an integropartial differential equation involving the new independent variable θ. This increases the complexity of the model but also yields certain insights as follows.

(1) Dichotomous branching has two effects: (a) it increases the density of apices; (b) it causes a *dispersal in orientations.* (In other words, the distribution $n(\cdot, \theta, \cdot)$ tends to spread in θ as if by diffusion: see the small angle approximation of the branching operator, given by (13).)

(2) Crosslinking selectively eliminates those apices moving "against the grain" (i.e., transverse to the orientation field).

These observations suggest the possibility of pattern formation in two-dimensional branching continua. The interplay between diffusion in θ, local autocatalysis (by branching), and inhibition by crosslinking would appear to predict that patterns could arise from angular instabilities of a homogeneous state. In the next section we describe a simplified space-independent set of equations, and demonstrate this property that results in the effect of orientation selection in a *YH* network.

5. Spatially homogeneous networks and θ instabilities. As a first step, consider a collection of filaments that are homogeneous in space and isotropic in orientation. For example, consider a broth made up of short lengths of filaments, where orientations are purely random, not the result of coherent growth. (See Fig. 3(a).) Since there is no front or spatial gradient of density, the spatial uniformity of this "network" will be unchanged by growth. However, since interconnections and branching events as

(a)

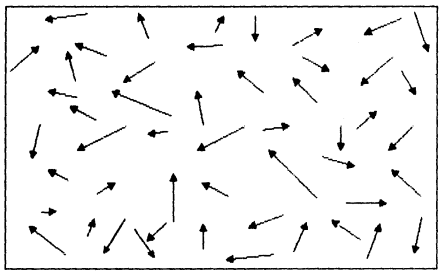

(b)

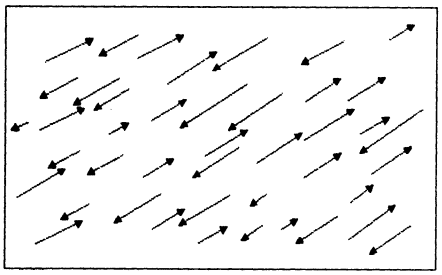

FIG. 3. *A spatially homogeneous "filament soup" in which orientations are initially random as shown in* (a) *will, as a result of interactions described in the model given by equations* (22a), (22b) *evolve into a collection of parallel branches shown in* (b).

well as death of filaments will take place, the initially uniform distribution of orientations will be affected by growth. To examine the consequences we explore the following model in which spatial dependence of the variables is omitted and equations are written in terms of $\rho(\theta, t)$ and $n(\theta, t)$.

For purposes of illustration we consider the case of *YH* branching networks. (The stability analysis is similar for the other cases.) Spatially homogeneous *YH* networks satisfy the equations

$$\frac{\partial \rho}{\partial t} = vn - \gamma\rho, \tag{22a}$$

$$\frac{\partial n}{\partial t} = \alpha(n_- - n + n_+) - \beta \int_{-\pi}^{\pi} K(\theta - \theta')\rho(\theta')\, d\theta'. \tag{22b}$$

These equations have isotropic (i.e., θ-independent) equilibrium solutions $(\rho_0, n_0) = (0, 0)$ and $(\bar{\rho}, \bar{n}) = (\alpha/\beta, \gamma\alpha/v\beta)$. Below we show that if the ratio μ/α is sufficiently small, then the homogeneous solution, $(\bar{\rho}, \bar{n})$ is unstable. The linearized equations for (22a), (22b) are:

$$\frac{\partial \rho}{\partial t} = vn - \gamma\rho, \tag{23a}$$

$$\frac{\partial n}{\partial t} = \alpha(n_- - 2n + n_+) - (\gamma\alpha/v) \int_{-\pi}^{\pi} K(\theta - \theta')\rho(\theta')\, d\theta'. \tag{23b}$$

The solutions to (23) are

$$[\rho(\theta, t), n(\theta, t)]^T = \begin{bmatrix} \rho_1 \\ n_1 \end{bmatrix} e^{il\theta} e^{\lambda t}, \tag{24}$$

where l is any integer, and $\{\lambda, [\begin{smallmatrix}\rho_1\\ n_1\end{smallmatrix}]\}$, is an eigenvalue-eigenvector pair for the 2×2 matrix:

$$\begin{bmatrix} -\gamma & v \\ -(\gamma\alpha/v)\hat{K}(l) & 2\alpha(\cos(l\varphi)-1) \end{bmatrix}. \tag{25}$$

In (25) the function $\hat{K}(l)$ is the Fourier transform of the function $K(\theta)$,

$$\hat{K}(l) = \int_{-\pi}^{\pi} e^{i\theta l} K(\theta)\, d\theta. \tag{26}$$

Since K is even, $\hat{K}(l)$ is real. For $K(\theta) = \frac{1}{4}|\sin(\theta)|$,

$$\hat{K}(l) = \begin{cases} 0, & l = 1, 3, 5, \cdots, \\ 1/(1-l^2), & l = 0, 2, 4, \cdots. \end{cases} \tag{27}$$

The eigenvalues of (25) will have negative real parts (and thus the equilibrium point will be stable) if the determinant is positive and the trace is negative. Clearly the latter condition will always hold since the trace $[2\alpha(\cos(l\varphi)-1)-\gamma]$ is always negative. If the determinant becomes negative, we can expect to see a loss of stability of the rest state as a real eigenvalue changes from negative to positive. Generically, we then expect bifurcation of small amplitude solutions that are proportional to $\cos(l\theta)$. The determinant of (25) is

$$\Delta(l) \equiv \alpha\gamma[2(1-\cos l\varphi) + \hat{K}(l)]. \tag{28}$$

For $K(\theta)$ as above, $\Delta(l)$ is positive for $l = 0, 1, 3, 5, \cdots$, but can be negative for $l = 2, 4, 6, \cdots$ provided $(1-\cos l\varphi)$ is sufficiently small. In particular, for stability we require

$$2(1-\cos l\varphi) > \frac{1}{(l^2-1)} \equiv f(l), \qquad l = 2, 4, 6, \cdots. \tag{29}$$

The function $f(l)$ is maximal when $l = 2$, (with $f(2) = \frac{1}{3}$.) Summarizing, we have found that for $K(\theta) = \frac{1}{4}|\sin(\theta)|$, the homogeneous solution is *stable* provided that

$$\cos 2\varphi < \tfrac{5}{6}. \tag{30}$$

If the above inequality is *not* satisfied, we expect to see inhomogeneous solutions bifurcating from the homogeneous state. The solutions will bifurcate stably only from the lowest $(l = 2)$ mode, since as $\Delta(l)$ decreases, the $l = 2$ mode bifurcates first. We can restate the stability criterion in terms of φ only. The result is that (30) is equivalent to

$$\varphi < \tfrac{1}{2}\arccos\tfrac{5}{6}, \quad \text{or} \quad \varphi < 0.29 \text{ radians} \approx 16.8°.$$

It follows that any branching network of the *YH* type will exhibit this type of orientation instability when the branching angle is smaller than 16.8°, regardless of all other parameter values, including the branching rate α, the rate of linking β, the rate of extension v, and the death rate γ.

In Fig. 4 we show the result of a numerical solution of (22a), (22b) for $\cos 2\varphi > \frac{5}{6}$. Starting from small perturbations of the homogeneous steady state, we observe that the initially random assortment of filament orientations gives rise to a pair of predominant directions, $\hat{\theta}$, and $\hat{\theta}+\pi$. Thus, starting from an unoriented mixture, instability gives rise to a network in which all filaments are aligned parallel to one another. The final network will have an appearance shown in Fig. 3(b).

The above results are not highly sensitive to the form of the kernel $K(\theta)$ chosen above. Key properties of this kernel necessary for a physically reasonable model for crosslinking are the following:

(i) $K(\pi-\theta)=K(\theta)$;

(ii) $K(-\theta)=K(\theta)$;

(iii) $K(\theta)$ is monotone increasing on $(0, \pi/2)$.

That is, $K(\theta)$ is maximal at $\pm\pi/2$ and symmetric about $\pm\pi/2$. These are physically reasonable requirements since the anastomosis should have its maximal effect when the branches are perpendicular but should not be sensitive to the absolute orientations of the branches.

Remark. We conjecture that for any $K(\theta)$ that has the above properties, the behavior will be qualitatively the same, that is, bifurcation will always occur first at $l=2$.

6. Spatially distributed networks. In the previous sections, we studied the behavior of networks without spatial structure. For spatially distributed networks growing in two dimensions, ρ and n, which are both functions of x, y, θ, and t, are described by (21).

Since these equations are rather complex, analytical results for the general case are difficult to obtain. Some general remarks, however, can be made on the basis of the equations themselves. We observe that (21b) is hyperbolic in the spatial variables x and y. Thus, the model is consistent with such spatial phenomena as propagating fronts and waves. It appears that no mechanism exists in these equations for generating instability of the uniform steady state to spatially nonuniform perturbations. This means that spatially periodic networks cannot be generated by the simple growth laws described in this paper. By implication, other mechanisms such as nonconstant extension rates, attraction to or repulsion from pre-existing density, or dependence on

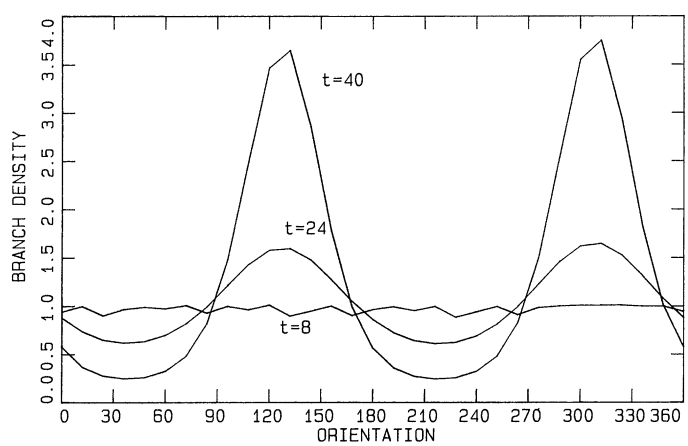

FIG. 4. *A spatially uniform network exhibits instability to random perturbations in the branch orientations. Starting close to a state in which all directions* $(0<\theta<360°)$ *are equally represented, two predominant directions that differ by* 180° *are formed. Equations* (22a), (22b) *were integrated with* $\alpha=1.2$, $\beta=5.0$, $\gamma=0.2$, $\varphi=.09$, $v=1.0$. *Shown are the distributions* $\rho(\theta, t)$ *at* $t=8$, 24, *and* 40 *units.*

other external influences must be responsible for spatial oscillations seen in some networks (for example, in fungi).

Next we turn to numerical solutions of several special cases in which the initial distribution has properties that reduce the dimensionality of the phenomenon.

6.1. Discrete equations. In carrying out numerical computations, we must return to a discrete formulation of the equations. The connection between the original discrete branching process and the discretized model is of some interest. In certain cases, chiefly when the branching angle is a rational divisor of 2π, $\varphi = 2\pi/m$, and when the initial distribution contains only branches oriented along directions $(2\pi/m)i$, $i = 1, 2, \cdots, \text{km}$, a finite set of discrete orientations are possible in the network. More generally, if φ is an irrational divisor of 2π, the orientation spectrum is continuous since in principle all orientations can be generated as a result of branching. In the latter case, discretization in angle is artificial, for the purposes of numerical analysis only.

In the following we define discrete variables as follows:

φ = the branching angle,

N = number of orientations in the discretized model,

$\Delta\theta = 2\pi/N$,

$\theta_j = j\Delta\theta$ = the jth orientation,

$\rho_j(x, y, t)$ = density of filaments oriented at angle θ_j counterclockwise from the x-axis at position (x, y) and time t,

$n_j(x, y, t)$ = density of tips whose direction of motion has orientation θ_j at position (x, y) and time t.

A discretized version of (21) is then

$$\frac{\partial \rho_j}{\partial t} = v n_j - \gamma \rho_j, \tag{31a}$$

$$\frac{\partial n_j}{\partial t} = -\nabla_h \cdot v_j n_j + \mathcal{D}(n_{j-1} - 2n_j + n_{j+1}) + n_j\left(\alpha - \beta \sum_{i=0}^{N-1} K(\theta_i - \theta_j)\rho_i\right), \tag{31b}$$

where $v_j = v(\cos\theta_j, \sin\theta_j)$, $\mathcal{D} = \alpha\varphi^2/(\Delta\theta)^2$, $\sum_{i=0}^{N-1} K(\theta_i) = 1$, ∇_h is a discrete spatial divergence operator, and $h = \Delta x = \Delta y$ is the spatial grid dimension.

6.2. Numerical simulations.

Case (i). *Initial growth along a single axis.* Consider the case in which $\partial n/\partial y|_{t=0} = 0$ and all branches are initially oriented along the x axis. An example of a network with this property would be an infinite array of equally spaced branches initially growing in parallel. (A second example would be that of equally spaced branches growing on the surface of a cylinder, parallel to the axial direction.) It is easy to verify that if the initial densities of ρ and n are uniform in the y direction, they will remain uniform under the dynamics. Therefore, we may set $\partial n/\partial y = 0$ in (31b) and the equations need only be integrated in the variables θ, x, and t.

Numerical integration of (31b) is carried out in two steps, each of increment $\frac{1}{2}\Delta t$: In the first step the diffusion operator in the theta direction is treated explicitly. In the second step, translation in the x-direction is carried out in the "upwind" direction. Since the velocity is proportional to $\cos\theta$, movement is forward for $|\theta| < \pi/2$ and in the reverse direction for $|\theta| > \pi/2$; this must be considered when integrating with respect to the spatial variable, since the direction of integration in the numerical simulation must match the direction of motion for stability.

Equations such as (21) will develop traveling wave solutions whose velocity exceeds v if the initial data is not of compact support (as discussed briefly in § 3). However, there are circumstances in which we are interested in studying the growth

of a network into a previously uncolonized region. To do so, it is necessary to place safeguards in the numerical code to ensure that numerical dissipation does not introduce finite densities at locations ahead of the margin of the network. Since the margin is predetermined to move at a constant rate v by virtue of the hyperbolic nature of (21), this can be done artificially by setting $\rho = n = 0$ at sites beyond the margin.

Equations (31) were integrated for $\Delta x = \Delta t = 0.1$, $\Delta\theta = 2\pi/N$, $N = 30$ on a domain of length $L = 50\Delta x$ with parameter values $\alpha = 0.5$, $\beta = 0.5$, $\gamma = 0.5$, and $v = 0.12$. Initially, branches and tips occupy only the two sites adjacent to $x = 0$ and are oriented parallel to the x-axis.

The domain is periodic in the θ direction. Because of the directions of motion along the x-axis, boundary conditions on the x variable are as follows:

$$n(0, \theta, t) = \begin{cases} n_0, & \theta = 0, \\ 0, & |\theta| < \pi/2, \end{cases} \tag{32}$$

$$n(L, \theta, t) = 0, \qquad |\theta| > \pi/2.$$

This means that there are always some apices growing from the origin, and that there are no tips growing in a reverse direction at the far boundary of the domain. Integration is halted when the growth margin first arrives at $x = L$.

Time behavior of the solutions was studied for a variety of branching angles, ranging from $\varphi = 0.1$ to $\varphi = 0.6$. Most of the interesting behavior was found in the range $0.2 < \varphi < 0.3$ and occurred during the time span $0 < t < 25$. By $t = 25$, characteristic patterns of growth were well established and continued to advance along the single space dimension (the x axis) without changing structure.

To present solutions graphically, we use a grey scale (with 20 grey levels) on an $x\theta$ coordinate system. The x axis is vertical (directed downwards) and the θ axis is subdivided into the regions $[-\pi, -\pi/2]$, $[-\pi/2, 0]$, $[0, \pi/2]$, $[\pi/2, \pi]$.) The densities of branches $\rho(x, \theta)$ are shown in a time sequence with $t = 5$, 10, 15, 20, and 25, starting at the top of the figure and continuing downwards. Shown in Figs. 5 and 6 are solutions for $\varphi = 0.2$ and $\varphi = 0.325$.

From these results, the following observations can be made. In the initial stages of growth, the patterns produced are circular or ellipsoidal in $x\theta$, since new orientations are introduced by branching. Branches growing parallel to the x axis, however, move fastest in the x direction. This tends to elongate the structure and gives rise to a leading margin.

In comparing Figs. 5 and 6 we observe that in both cases some retrograde motion occurs in the networks. However, for $\varphi = 0.2$ in Fig. 5 this is apparent only in the rearmost section of the network, while for $\varphi = 0.325$ in Fig. 6 it occurs at locations close to the leading edge. A second remark is that orientations tend to be sharply defined throughout most of the network in Fig. 5 and diffuse in Fig. 6. This pattern continues when integration is carried out for longer times.

Third, the angular profile is constant over the middle half of the network by $t = 25$ in Fig. 5, whereas, in Fig. 6, the angular profile gradually broadens toward the rear of the structure. This phenomenon can be explained as a spatially-propagating version of the orientation selection effect described in § 5. That is, in networks with crosslinkage and small branching angles, there is a tendency for alignment along some predominant direction. Since initially the networks in these simulations were directed along the x axis, this direction is a preferred one, and thus forms the chief orientation axis in Fig. 5.

When $\varphi = 0.2$, orientations that are at angles close to $\pi/2$ are rapidly eliminated in the front of the network and are thus not present in Fig. 5. The "tails" at the rear

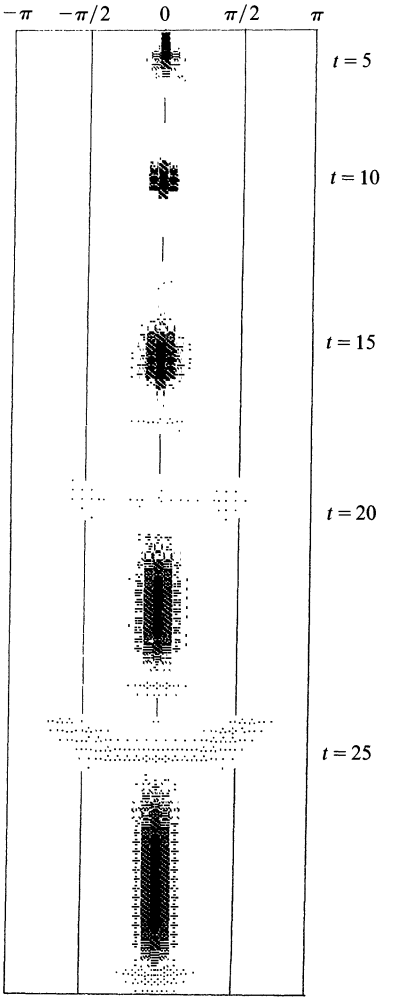

FIG. 5. *A sequence of five shapes formed in development of a network that initially consists of a collection of branches parallel to the x axis. Shown is the density of branches at intervals of 5 time units starting at* $t = 5$. *The branching angle is* $\varphi = 0.2$; *other parameters used are* $\alpha = \beta = \gamma = 0.5$, $v = 0.12$. *See the text for details.*

of the structure are vestiges, stemming from the fact that initially the network is not sufficiently dense for crosslinking to eliminate large angles. Some branches also continue to "escape" to the rear later in parts of the network where the alignment is not yet established.

Figure 7 demonstrates the effect of varying φ on the shape of the networks at $t = 35$. It is apparent that the transition from sharp to diffuse orientations occurs roughly between $\varphi = 0.24$ and $\varphi = 0.28$ (close to the bifurcation value found in § 5). The angular profiles of such networks at several locations are shown below their respective grey-scale plots. Figure 8, in which the profiles at the margin are directly compared, gives evidence of the widening that occurs when φ is increased.

Case (ii). *Symmetric networks and rational branching angles.* We now consider the special case that the branching angle $\varphi = 2\pi/N$. If initially the only orientations in the network are $\theta_j = 2\pi j/N = \varphi j$, $j = 1, 2, \cdots, N$, then only these orientations will

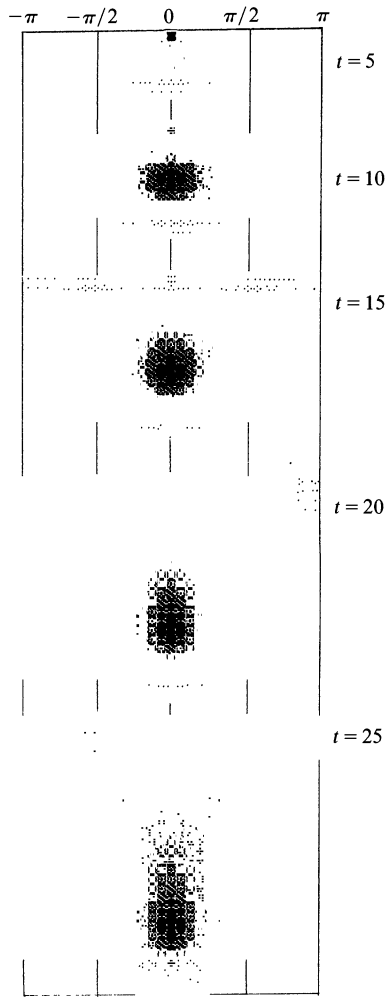

FIG. 6. *Five shapes in the development of the same network but with* $\varphi = 0.325$. *In Figs.* 5 *and* 6 *the apex originally at* $(0, 0)$ *remains at* $(0, 0)$.

be present in the network. Then equations corresponding to (21) are:

$$\frac{\partial \rho_j}{\partial t} = v n_j - \gamma \rho_j, \tag{33a}$$

$$\frac{\partial n_j}{\partial t} = -\nabla \cdot (v_j n_j) + \alpha(n_{j-1} - n_j + n_{j+1}) - \beta n_j \sum_{i=0}^{N-1} K(\theta_i - \theta_j)\rho_i, \tag{33b}$$

where

$$\mathbf{v}_j = \mathbf{v}(\cos\theta_j, \sin\theta_j). \tag{33c}$$

These equations may be numerically integrated but the computations are quite lengthy since the problem is effectively $2N$-dimensional. We can eliminate all but one of the N pairs of equations by exploiting certain symmetries in (33).

Suppose that we start with initial data for (33) having the following radial symmetry:

$$z_0(x, y, 0) = z_j(\mathcal{R}_j\{x, y\}, 0), \tag{34}$$

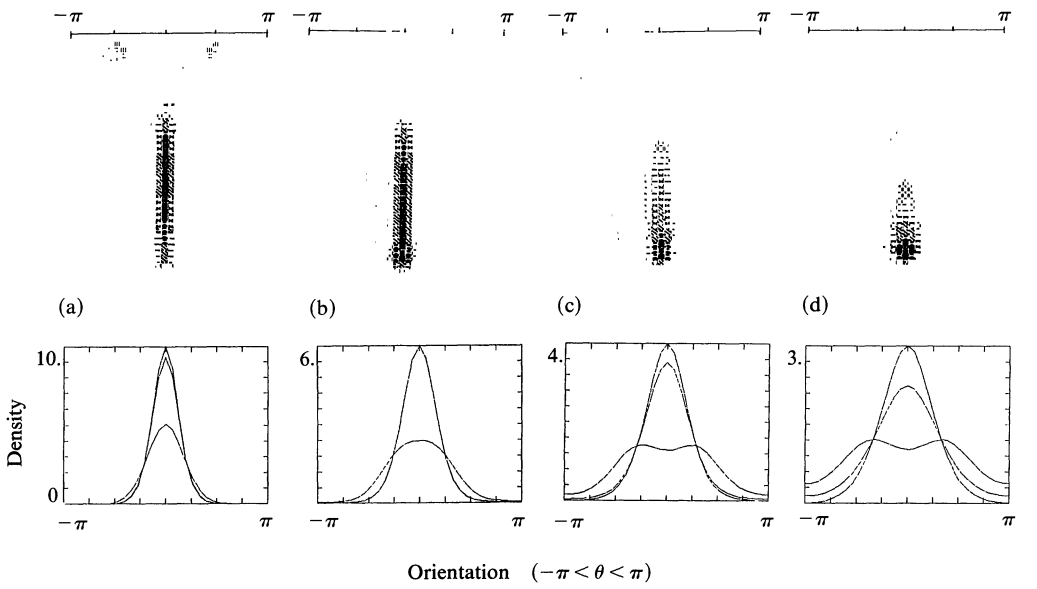

FIG. 7. *A comparison of the final densities of networks (at $t = 35.$) obtained as the branching angle is varied. Shown are four cases, for $\varphi = 0.2$, 0.24, 0.28, and 0.325. The plots shown below the corresponding grey scales represent the density of branches of a given orientation, θ, $-180 < \theta < 180$ at $x = L/4$, $L/2$, and $3L/4$, where L is the length of the network. In each case, the lowest curve represents density closest to the origin. In* (a) *the highest curve is density at $x = L/2$. In* (b) *the curves for $x = L/2$ and $x = 3L/4$ are identical. In* (c) *and* (d) *the roles are reversed, with highest density at $x = 3L/4$.*

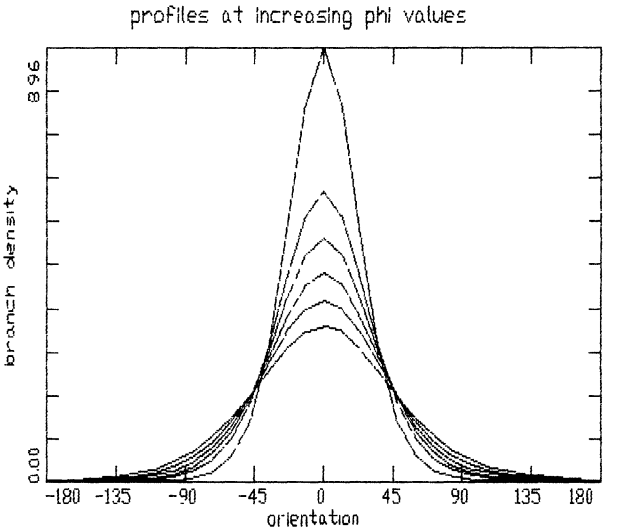

FIG. 8. *The density of branches as a function of orientation at $x = 3L/4$ (where L is the length of network) for $\varphi = 0.2$ (tallest peak), 0.24, 0.26, 0.28, 0.3, and 0.325 (lowest peak). Increasing the branching angle tends to broaden the distribution of branch orientations.*

where z is either ρ or n and $\mathcal{R}_j$ is the rotation matrix

$$\mathcal{R}_j = \begin{bmatrix} \cos\theta_j & -\sin\theta_j \\ \sin\theta_j & \cos\theta_j \end{bmatrix}. \tag{35}$$

Let

$$(\hat{x}_j, \hat{y}_j) = \mathcal{R}_j\{x, y\}.$$

Then

$$(\hat{x}_j, \hat{y}_j) = (x\cos\theta_j - y\sin\theta_j,\ x\sin\theta_j + y\cos\theta_j) \tag{36}$$

is a position obtained by rotating the axes by an amount θ_j. Equation (34) means that at $t=0$, the density of j-oriented elements at position $(\hat{x}_j, \hat{y}_j)$ is identical with the density of elements of zero orientation at a position (x, y). Initial conditions that satisfy this symmetry include those for which there is a homogeneous distribution of branching angles at each spatial point (constant initial conditions), those whose contours resemble N-sided snowflake patterns, and those concentrated at the origin $(x, y) = (0, 0)$. In the Appendix it is shown that (33) preserves this symmetry. If we restrict our attention to symmetric solutions, we need only solve for $n_0(x, y, t)$ and $\rho_0(x, y, t)$. The resulting symmetric two-dimensional (instead of $2N$-dimensional) hyperbolic system is

$$\frac{\partial \rho_0}{\partial t} = v n_0 - \gamma \rho_0, \tag{37a}$$

$$\begin{aligned} \frac{\partial n_0}{\partial t} + v\frac{\partial n_0}{\partial x} &= \alpha[n_0(\mathcal{R}_1\{x, y\}) + n_0(\mathcal{R}_{-1}\{x, y\}) - n_0(x, y)] \\ &\quad - \beta n_0(x, y)\sum_{i=0}^{N-1} K(\theta_i)\rho_0(\mathcal{R}_i\{x, y\}), \end{aligned} \tag{37b}$$

where we take

$$K(\theta) = C|\sin(\theta)|, \tag{37c}$$

with C chosen so that

$$C\sum_{i=0}^{N-1} |\sin\varphi_i| = 1. \tag{37d}$$

Because of the symmetry properties discussed above, average densities can be defined by summing over the N corresponding positions (obtained by rotation through angles θ_j, $j = 1, \cdots, N$), a process equivalent to summing over all discrete orientations at a given spatial position. Thus, average densities are defined by

$$\bar{\rho}(x, y, t) \equiv \frac{1}{N}\sum_{i=0}^{N-1} \rho_0(\mathcal{R}_i\{x, y\}, t), \tag{38a}$$

$$\bar{n}(x, y, t) \equiv \frac{1}{N}\sum_{i=0}^{N-1} n_0(\mathcal{R}_i\{x, y\}, t). \tag{38b}$$

The solution to (37) yields values for $[\rho_0(x, y, t), n_0(x, y, t)]$; the densities of the other orientations can then be found by applying the transformation (34). Equations (37) are analyzed numerically on a square domain $\Omega = [-3, 3]\times[-3, 3]$ with Dirichlet boundary conditions. The domain Ω is discretized into a grid of 61×61 points and the spatial derivative $\partial n_0/\partial x$ is approximated by an upwind differencing scheme for numerical stability. We use an angle discretization of $N = 18$. Integration of the equations is halted as soon as the growth reaches the boundaries of the domain.

To compare the wavelike behavior of networks with and without compact support, we examined two cases. In the first, initial data had small but nonzero densities throughout the domain, with a peak at the origin, and with a uniform initial angular distribution. The parameters had values $\Delta x = \Delta t = 0.1$, $\alpha = 1.0$, $\beta = 1.0$, $v = 0.05$, $\gamma = 0.05$. This situation is representative of a network in which exploratory branches have already been established, and in which a wave of branching then takes place. Below we describe properties of the numerical solutions by displaying graphs of densities averaged over all orientations, as well as proportions of filaments aligned in a given direction (at angle $\theta = 0$). Figure 19 depicts the time evolution of solutions to (37).

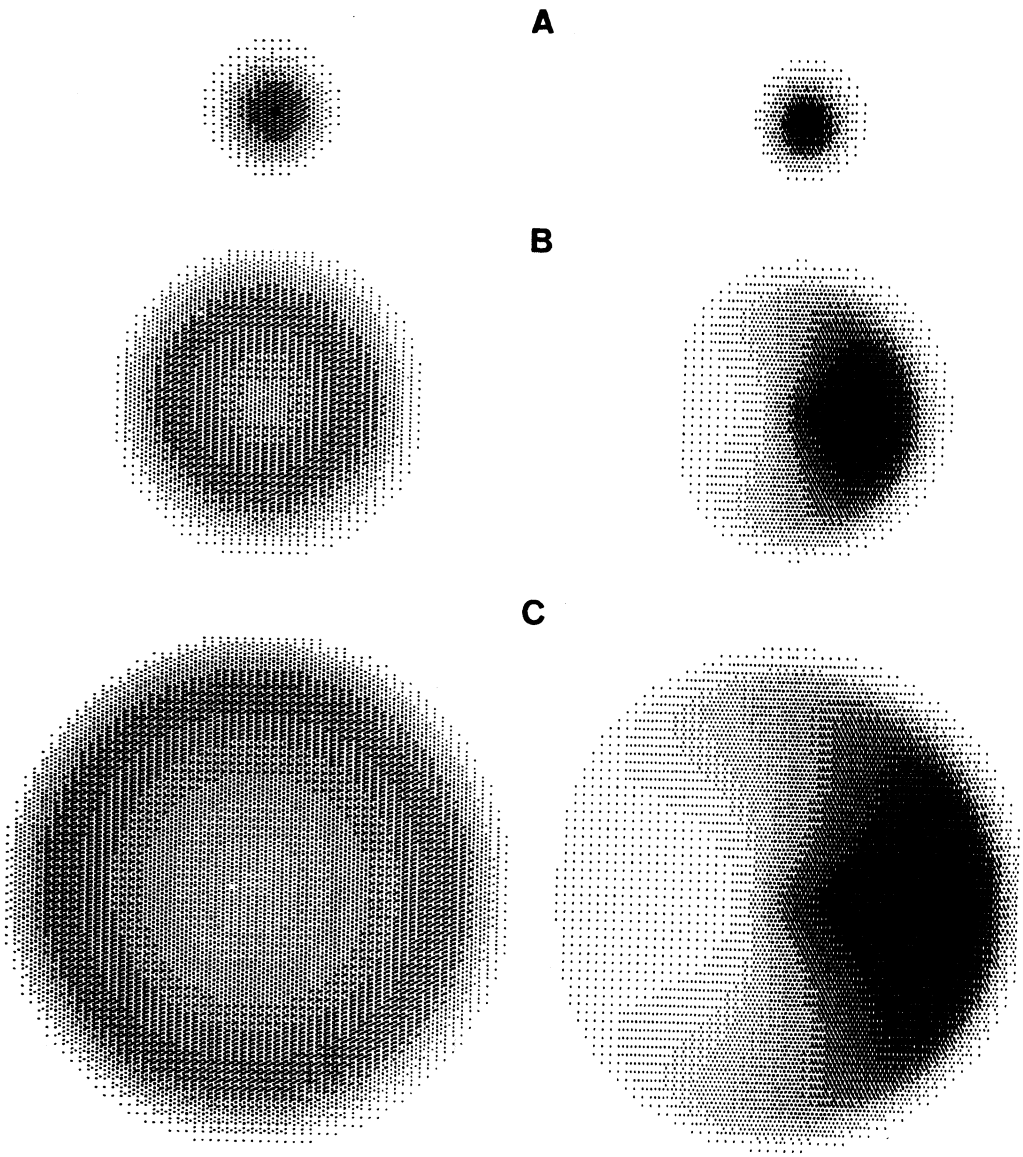

FIG. 9. *Time evolution of the discrete angular symmetric model given by equations* (37). *The density of filaments averaged over all orientations* $\bar{\rho}$ *is shown as a function of position* (x, y) *on the left-hand side. The proportion of filaments parallel to the x axis* ρ_0 *at a given position* (x, y) *is shown on the right.* (A) $t = 8$, (B) $t = 16$, (C) $t = 24$. *See the text for details of initial conditions and parameter values.*

On the left, the average filament density $\bar{\rho}(x, y, t)$ is displayed. On the right, the intensity of shading represents the proportion of filaments at a given position whose orientation angle is $\theta_0 = 0$ (i.e., filaments directed toward the positive x axis $\rho_0(x, y, t)$). The sequence of three frames from top to bottom depicts the densities at three consecutive times, $t = 8, 16, 24$. Observe that close to the positive x axis, a very high proportion of filaments are oriented at 0°, since this corresponds to motion radially outward. Along the negative x axis, a small fraction of filaments are oriented at $\theta = 0$, corresponding to those branches moving in the reverse direction (toward the origin). The same figure may be used for viewing the proportion of density oriented at any angle $\theta_j = 2\pi j/18$ radians $= j \cdot 20°$. To do so, rotate the figure by θ_j. The density of shading along the new x axis then represents the proportion of branches oriented at angle $-\theta_j$ along the old x axis. (For example, the shading density along a radius of the figure at 40° to the x axis represents the fraction of branches oriented at angle −40° along the x axis.)

Further properties of these solutions are displayed in Figs. 10–12. In Fig. 10, we depict the spatial profiles of the average densities, $\bar{\rho}$, $\bar{n}$ along the x axis at several

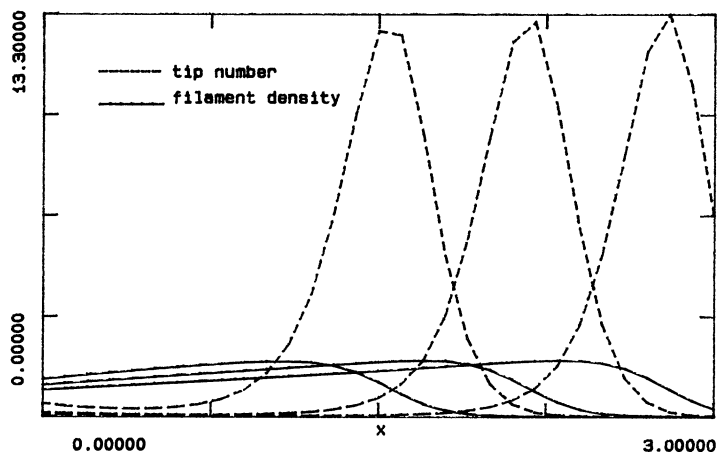

FIG. 10. *Profiles of the average densities as functions of distance along the positive x axis*: $\bar{\rho}(x, 0, t)$ (*solid curves*), *and* $\bar{n}(x, 0, t)$ (*dashed curves*) *at* $t = 16, 20, 24$.

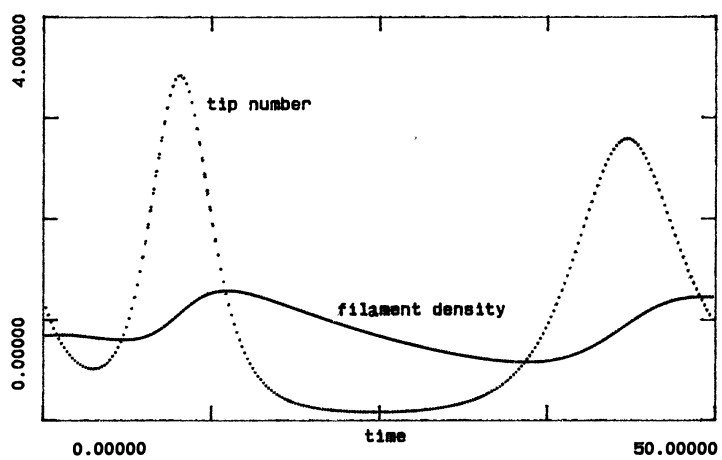

FIG 11. *Time evolution of the average densities at the origin*: $\bar{\rho}(0, 0, t)$ (*solid curve*) *and* $\bar{n}(0, 0, t)$ (*dotted curve*).

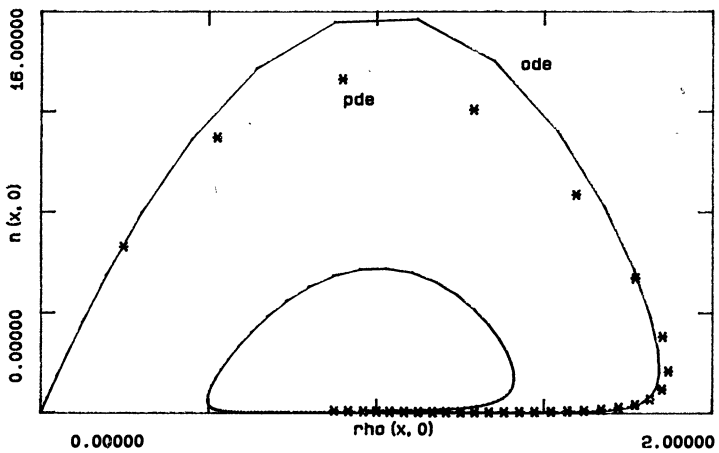

FIG. 12. *Comparison of the predictions of equations* (37) *with predictions of the ordinary differential equations* (6) *shown in a ρn phase plane diagram. The solid line depicts a positive heteroclinic trajectory of* (39) *that represents a bounded traveling wave solution of equations* (6). *The *'s represent pairs of values* $[\bar{\rho}(x, 0, t), \bar{n}(x, 0, t)]$ *for* $t = 16$ *and positive values of* x.

different times. There is clearly a well-defined traveling wave moving outward from the center. From the numerical simulations we observe an approximate wave velocity of 0.15 for $t > 10$. This velocity depends on the form of the initial conditions but is always larger than the absolute velocity of the apices, v (here, equal to 0.05), for reasons that were previously discussed, and that are detailed further below. Figure 11 shows the time evolution of the average filament density and tip number at the center of the field as functions of time. We observe an oscillatory approach to the equilibrium values.

To understand the traveling wave behavior of the average densities in this setting we examine a further simplification of (37). If we apply the transformation (34) to (37) and average over all orientations, the averages $(\bar{\rho}, \bar{n})$ satisfy

$$\frac{\partial \bar{\rho}}{\partial t} = v\bar{n} - \gamma\bar{\rho}, \qquad \frac{\partial \bar{n}}{\partial t} + v\frac{\partial \bar{n}}{\partial x} = \alpha\bar{n} - \beta\bar{n}\sum_{i=0}^{N-1} K(\varphi_i)\rho_0(\mathcal{R}_i\{x, y\}). \tag{39}$$

If we approximate the sum in (39) by the average, $\bar{\rho}(x, y)$, (39) becomes

$$\frac{\partial \bar{\rho}}{\partial t} = v\bar{n} - \gamma\bar{\rho}, \qquad \frac{\partial \bar{n}}{\partial t} + v\frac{\partial \bar{n}}{\partial x} = \bar{n}(\alpha - \beta\bar{\rho}). \tag{40}$$

If we look for y-independent solutions to (40) we observe that this averaged problem reduces to the one space-dimensional model of equations (1)–(3) that has been analyzed in § 3. Thus, for initial conditions with noncompact support, traveling wave solutions are to be expected. This observation explains several aspects of the simulation of (37). For the parameters used, $[\alpha/\beta, \alpha\gamma/\beta v]$ is a spiral. This explains the oscillatory behavior in Fig. 11. Furthermore, the required connections do not occur if $c < v$, which explains why the velocity of the front in these simulations is greater than the branch extension rate.

In Fig. 12, we compare the solutions to the shooting problem (6) with the solutions to the problem (37) with all parameters as above and $c = 0.15$. The two are remarkably close given the crudeness of our approximation (the approximation of the weighted sum in (39) by the average), thus reinforcing the conclusion that the basic wavelike

behavior of solutions to the one-dimensional network model appear in higher dimensions as well.

7. Discussion. The main emphasis of this paper is on properties of two-dimensional networks that stem from an interplay of branching, which results in an enhanced potential for growth, and crosslinking, which has the opposite effect. While many real networks are spatially discrete, the continuum models derived here give us tools for analyzing and understanding the way that simple networks develop. Using such models, we have addressed questions about the shapes and internal structure (distribution of orientations) of such networks, and the rates with which networks grow and expand in one and two dimensions.

To place this theory in the context of other work on branching structures, it is worth commenting on several previous investigations. In many of these, branching patterns have been explored with an emphasis primarily on classification, numbering of the structures (e.g., [21], [14], [22], [11], [17]) and topological analysis [4]. Few studies, if any, have dealt with the mechanisms responsible for the patterns. Discrete simulations were pioneered by Cohen [5] and later applied to model systems such as tree canopies, [13], plant architecture [3], [19], and fungal colonies [15]. Reviews can be found in [23] and [18]. Most studies have been based on computer simulations without accompanying mathematical analysis. Furthermore, the effects of crosslinking have not been thoroughly investigated in these studies.

Several directions can be identified for extension of these models. First, it is of interest to address changes in orientations of branch tips that result from attraction (chemotaxis) toward high concentrations of diffusible substances, or from avoidance of crowding. Second, the effects of nonconstant rates of branching and crosslinking should be considered. Third, distributions of branching angles and branching types should be explored.

While networks arise from many distinct processes and have diverse functions in nature, their predominance in biological, physical, and chemical systems is striking. It may be reasonable to believe that many of the regulation and pattern formation phenomena in these various examples are related, and would therefore be amenable to a theoretical treatment related to the one outlined in this paper.

Appendix. Preservation of symmetry under the dynamics. Consider initial densities having the symmetry properties given in (34). Since spatial derivatives interact with the rotation operator, the flux term, $(v_j \cdot \nabla n_j)$ must be considered. Suppose that

$$n_0(x, y, t) = n_j(\hat{x}_j, \hat{y}_j, t);$$

then

$$\begin{aligned}\frac{\partial[n_0(x, y, t)]}{\partial x} &= \left(\frac{\partial \hat{x}_j}{\partial x}\right)\frac{\partial[n_j(\hat{x}_j, \hat{y}_j)]}{\partial \hat{x}_j} + \left(\frac{\partial \hat{y}_j}{\partial x}\right)\frac{\partial[n_j(\hat{x}_j, \hat{y}_j)]}{\partial \hat{y}_j} \\ &= \cos\theta_j \frac{\partial[n_j(\hat{x}_j, \hat{y}_j)]}{\partial \hat{x}_j} + \sin\theta_j \frac{\partial[n_j(\hat{x}_j, \hat{y}_j)]}{\partial \hat{y}_j} \\ &= (\cos\theta_j, \sin\theta_j) \cdot \nabla n_j \\ &= \left(\frac{1}{v}\right)\nabla \cdot (v_j n_j).\end{aligned}$$

Thus, the equations preserve symmetry at each time step.

REFERENCES

[1] W. ALT, *Biased random walk models for chemotaxis and related diffusion approximations*, J. Math. Biol., 9 (1980), pp. 147–177.

[2] D. BALDING AND D. L. S. MCELWAIN, *A mathematical model of tumor-induced capillary growth*, J. Theoret. Biol., 114 (1985), pp. 53–73.

[3] A. D. BELL, D. ROBERTS, AND A. SMITH, *Branching patterns: the simulation of plant architecture*, J. Theoret. Biol., 81 (1979), pp. 351–375.

[4] M. BERRY AND P. M. BRADLEY, *The application of network analysis to the study of branching patterns of large dendritic fields*, Brain Res., 109 (1976), pp. 111–132.

[5] D. COHEN, *Computer simulation of biological pattern generation processes*, Nature, 216 (1967), pp. 246–248.

[6] L. EDELSTEIN, *Growth and morphogenesis with plants and fungi as examples*, Ph.D. thesis, Weizmann Institute, Revohot, Israel, 1981.

[7] ———, *The propagation of fungal colonies; a model for tissue growth*, J. Theoret. Biol., 98 (1982), pp. 679–701.

[8] L. EDELSTEIN, Y. HADAR, I. CHET, Y. HENIS, AND L. A. SEGEL, *A model for fungal growth applied to Sclerotium rolfsii*, J. Gen. Microbiol., 129 (1983), pp. 1873–1881.

[9] L. EDELSTEIN AND L. A. SEGEL, *Growth and metabolism in mycelial fungi*, J. Theoret. Biol., 104 (1983), pp. 187–210.

[10] W. S. GLOCK, *The development of drainage systems: a synoptic view*, Geog. Rev., 21 (1931), pp. 475–482.

[11] K. GULL, *Mycelial branch patterns of Thamnidium elegans*, Trans. Br. Mycol. Soc., 64 (1975), pp. 321–362.

[12] L. HOLLIDAY AND I. M. WARD, *A general introduction to the structure and properties of oriented polymers* (Chapter 1), in Structure and Properties of Oriented Polymers, I. M. Ward, ed., John Wiley, New York, 1975.

[13] H. HONDA, *Description of the form of trees by the parameters of the tree-like body: effects of the branching angle and the branch length on the shape of the tree-like body*, J. Theoret. Biol., 31 (1971), pp. 331–338.

[14] K. HORSFIELD, *Some mathematical properties of branching trees with application to the respiratory system*, Bull. Math. Biol., 38 (1976), pp. 305–315.

[15] S. A. HUTCHINSON, P. SHARMA, K. R. CLARKE, AND I. MACDONALD, *Control of hyphal orientation in colonies of Mucor hiemalis*, Trans. Brit. Mycol. Soc., 75 (1980), pp. 177–191.

[16] S. S. LABANA, S. NEWMAN, AND A. J. CHOMPFF, *Chemical effects on the ultimate properties of polymer networks in the glassy state*, in Polymer Networks; Structure and Mechanical Properties, A. J. Chompff and S. Newman, eds., Plenum Press, New York, 1971.

[17] L. B. LEOPOLD, *Trees and streams: the efficiency of branching patterns*, J. Theoret. Biol., 31 (1971), pp. 339–354.

[18] N. MACDONALD, *Trees and Networks in Biological Models*, John Wiley, New York, 1983.

[19] K. J. NIKLAS, *Computer-simulated plant evolution*, Scientific American, 254 (1986), pp. 78–86.

[20] S. RAMON-CAJAL, *Histology*, William Wood, Baltimore, 1933.

[21] F. J. ROHLF, *Numbering binary trees with labeled terminal vertices*, Bull. Math. Biol., 45 (1983), pp. 33–40.

[22] J. VAN PELT AND R. W. H. VERWER, *The exact probabilities of branching patterns under terminal and segmental growth hypotheses*, Bull. Math. Biol., 45 (1983), pp. 269–285.

[23] D. M. WALLER AND D. A. STEINGRAEBER, *Branching and modular growth: theoretical models and empirical patterns*, in Population Biology and Evolution of Clonal Organisms, J. B. C. Jackson, L. W. Buss, and R. E. Cook, eds., Yale University Press, New Haven, CT, 1985, pp. 225–257.